Article

Revisiting the Stereodetermining Step in Enantioselective Iridium-Catalyzed Imine Hydrogenation

Brandon Tutkowski, Sutthichat Kerdphon, Elaine Lime, Paul Helquist, Pher G. Andersson, Per-Ola Norrby, and Olaf Wiest

ACS Catal., **Just Accepted Manuscript** • DOI: 10.1021/acscatal.7b02386 • Publication Date (Web): 01 Dec 2017

Revisiting the Stereodetermining Step in Enantioselective Iridium-Catalyzed Imine Hydrogenation

Brandon Tutkowski,[a] Sutthichat Kerdphon,[b] Elaine Limé,[c] Paul Helquist,[a] Pher G. Andersson,[b] Olaf Wiest*,[a,d] Per-Ola Norrby[a,c]

[a]Department of Chemistry and Biochemistry, University of Notre Dame, Notre Dame, Indiana 46556. Email: owiest@nd.edu

[b]Arrhenius Laboratory, Department of Organic Chemistry, and Berzelii Centre EXSELENT on Porous Materials, Department of Materials and Environmental Chemistry, Stockholm University, SE-106 91 Stockholm, Sweden. Email: Pher.Andersson@su.se

[c]Pharmaceutical Development, AstraZeneca, Pepparedsleden 1, SE-431 80 Mölndal, Sweden. Email: per-ola.norrby@astrazeneca.com

[d]Laboratory of Computational Chemistry and Drug Design, School of Chemical Biology and Biotechnology, Peking University, Shenzhen Graduate School, Shenzhen 518055, China

Keywords

Imine hydrogenation, iridium, phosphine-oxazoline, mechanistic studies, stereoselectivity, density functional theory

Table of Contents Graphic

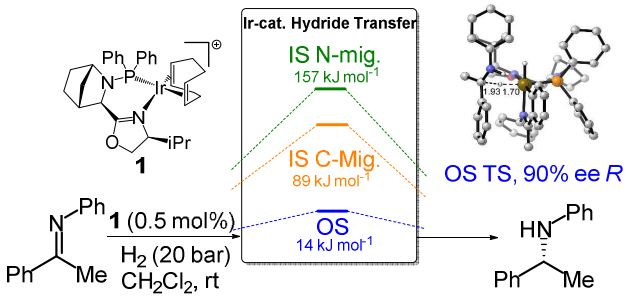

Abstract

The mechanism of the iridium-catalyzed asymmetric hydrogenation of prochiral imines has been investigated for an experimentally relevant ligand-substrate combination using DFT calculations. The possible stereoisomers of the stereodetermining hydride transfer transition state were considered for four possible hydrogenation mechanisms starting from the recently disclosed active catalyst consisting of iridium phosphine-oxazoline with cyclometalated imine substrate. The hydrogenation was found to proceed via an outer sphere pathway. The transition state accurately describes the experimental observations of the active catalyst and provides a

structural rationale for the high stereoinduction despite the lack of direct interaction points in the outer-sphere mechanism. The predicted enantioselectivity was consistent with experimental observations. Experimental studies support the hypothesis that the iridacycle forms spontaneously and functions as the active catalyst in the hydrogenation.

Introduction

The asymmetric hydrogenation of imines is an important method in the field of asymmetric synthesis. The chiral amine products of such a reaction are widely used as building blocks in the fine chemical and pharmaceutical industries.[1] Based on the seminal work of Crabtree in the late 1970's,[2] Pfaltz and coworkers developed an iridium complex with a chelating phosphine-oxazoline, or PHOX, ligand.[3] Since their initial utilization by Pfaltz, PHOX ligands have been used extensively in the asymmetric hydrogenations of both imine and olefin substrates.[1b,4] In subsequent work, Pfaltz and coworkers used NMR and DFT studies of Ir(phosphine-oxazoline)dihydride complexes to show that the complexes preferred a configuration with the hydrides *cis* to each other and one of them *trans* to the coordinating nitrogen in the oxazoline ring.[5] These studies also emphasized the importance of calculating the complete chiral ligand, rather than smaller model complexes, as the structure of the ligand controls the outcome of the enantiomeric product by both steric and electronic factors.

Many factors have been determined to be involved in the enantioselectivity of the reaction,[3] not the least of these being the choice of substituents on the phosphine-oxazoline ligand. While no clear trends in enantioselectivity have been elucidated for the substituents on phosphine, the substituent in the 5'-position on the oxazoline has been shown to control both enantioselectivity and reactivity. A ligand with an isopropyl (*i*Pr) group at this position was found to be most selective, while ligands with an isobutyl (*i*Bu) or phenyl group gave both lower conversion and lower enantioselectivity. The selectivity is also dependent on the imine substrate, with bulky and flexible substituents generally giving lower enantioselectivities.

Based upon earlier work where similar catalytic systems have been used to hydrogenate alkenes, quadrant models have been developed to predict the reaction enantioselectivity.[6] It is interesting to note that, for a given ligand, similarly substituted alkenes and imines can form products of opposite absolute configurations.[7] This indicates that even if there could be parallels between the mechanisms, the stereodetermining step for the two substrates must differ. Solvent and additives have also been found to influence the enantioselectivity, with dichloromethane or toluene being the best choice for acyclic imines.[8] Strongly coordinating solvents or additives can reduce enantioselectivity significantly,[9] with one possible explanation being that these solvents

block a contact point between substrate and metal. Another factor that might influence the enantioselectivity is the potential *E*/*Z* isomerization of the substrate, a factor that is not easily controlled. Based on the quadrant models, the *E*- and *Z*-isomers should interact differently with the catalyst, and the *E*/*Z* ratio should then be expected to have an effect on the enantiomeric excess (%*ee*). However, in studies where isomer mixtures of imines have been used, high enantioselectivities have still been achieved. This has led to the conclusion that mainly one imine isomer is reduced, and that imine isomerization is fast, keeping the *E*/*Z* ratio constant.[9a,10]

Because of these different observations, it is clear that the mechanism for the iridium-catalyzed imine hydrogenation is different from the Ir(III)/Ir(V) cycle which is widely accepted for alkene hydrogenation with P,N-ligands.[11] This discrepancy has inspired a number of studies on a range of different systems. Oro and coworkers have performed detailed studies of a system with a monodentate phosphine ligand and have found that the active catalyst also incorporates a coordinated aniline obtained from hydrolyzed imine substrate.[12] The resulting catalyst follows the now accepted pathway common to transfer hydrogenation catalysts,[13] with coupled transfer of a proton from the aniline and a hydride from iridium. The relationship of this mechanism to the Pfaltz PHOX system is, however, unclear.

Several other mechanisms have been proposed for Ir catalysts, covering inner- and outer sphere mechanisms and Ir(I)/Ir(III), Ir(III), and Ir(III)/Ir(V) cycles.[8,14] For the case of P,N-ligands, a detailed DFT study of the Pfaltz PHOX system[3] was performed by Hopmann and Bayer.[15] They investigated several mechanistic proposals for both alkene and imine hydrogenation at the B3LYP/6-311G**, LANL2DZ level of theory. For imine hydrogenation, the preferred rate- and selectivity-determining step is an outer sphere transfer of a hydride from a neutral Ir(III) trihydride complex to a cationic iminium ion. This is noteworthy because having only one strong contact (the Ir-H-C vector), it is different from typical enantioselective catalysts where multiple strong interactions are generally needed to achieve high selectivity. For example, the selectivity-determining step in inner sphere alkene hydrogenations can be a migratory insertion where the alkene is held rigidly by simultaneous contact with the metal and the hydride.[11a] Likewise, in outer sphere transfer hydrogenation reactions, the substrate is held in one position by simultaneous transfer of a proton and hydride from the active catalyst.[13,16]

Similar mechanistic proposals for imine hydrogenation using H_2 were invalidated by the surprising finding that upon exposing a dihydride complex of an iridium-PHOX precursor to an imine substrate under hydrogenation conditions, rapid formation of an iridacycle analogous to complex **2** in **Scheme 1** (*vide infra*) occurred.[17] Detailed experiments, including the collection of crystal structures showing the imine substrate cyclometalated to iridium, demonstrated that this

iridacycle is the active catalyst in the hydrogenation of acetophenone-derived imines. It was also shown that cyclometalation with one imine can change the selectivity in the reaction with another imine. An iridacycle has since been invoked as the active catalyst in an iridium-catalyzed transfer hydrogenation of imines.[18] Current published mechanistic proposals for iridium-PHOX catalyzed imine hydrogenations[15] do not include an iridacycle as the active catalyst. We decided to revisit the proposed reaction mechanisms for the imine hydrogenation in order to gain an understanding of the pathway for a pre-catalyst complex containing an aminophosphine-oxazoline ligand with a 2-azanorbornane backbone developed by Andersson and co-workers, **1**, which provided high *ee* values (**Figure 1**).[19] Because cyclometalation clearly changes the catalyst, we took a step back from previously published mechanisms and considered both inner and outer sphere mechanisms involving the iridacycle as the active catalyst. The goal of these studies was to elucidate the basis of stereoinduction of the imine hydrogenation catalyzed by **1** involving the iridacycle.

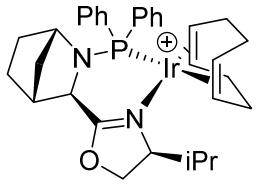

1

Figure 1. The iridium pre-catalyst with phosphine-oxazoline ligand studied in this work.

Results and Discussion

We considered the four potential mechanisms involving an iridacycle as the active catalyst shown in **Scheme 1**. These mechanisms were an outer sphere Ir(III) pathway, an inner sphere pathway through a heptacoordinate Ir complex, an inner sphere C-migration pathway, and an inner sphere N-migration pathway all involving iridacycle **2** as the active catalyst. The mechanisms investigated in this work are analogous to those investigated by Hopmann and Bayer, but involving an iridacycle complex rather than a di- or trihydride as the active catalyst.

The outer sphere mechanism begins with the binding of H_2 to an open coordination site of the catalyst. Proton transfer to the unbound imine substrate occurs, followed by hydride transfer and extrusion of product, completing the catalytic cycle. By contrast, the inner sphere mechanisms all include an imine substrate bound to the metal during the stereodetermining hydride transfer step. The inner sphere mechanism through a heptacoordinate complex has proton transfer to the substrate nitrogen occurring before hydride transfer. The C- and N-migration pathways involve hydride transfer to the substrate occurring before proton transfer. In

the C-migration pathway, hydride transfer occurs to the imine carbon of the substrate, leading to a complex with a negatively charged nitrogen bound to iridium. In the N-migration pathway, hydride transfer occurs to the nitrogen of the substrate, leading to a complex with a carbanion bound to iridium. As shown, the active catalyst in all mechanisms is an iridacycle with H_2 π-bound to iridium in what would otherwise be an empty coordination site. Hopmann and Bayer found that replacing a molecule of bound solvent with H_2 in this site of their catalyst had little impact on the relative energies of the final structures. For the sake of simplicity, we decided to use structures with H_2, rather than solvent, bound in this site.

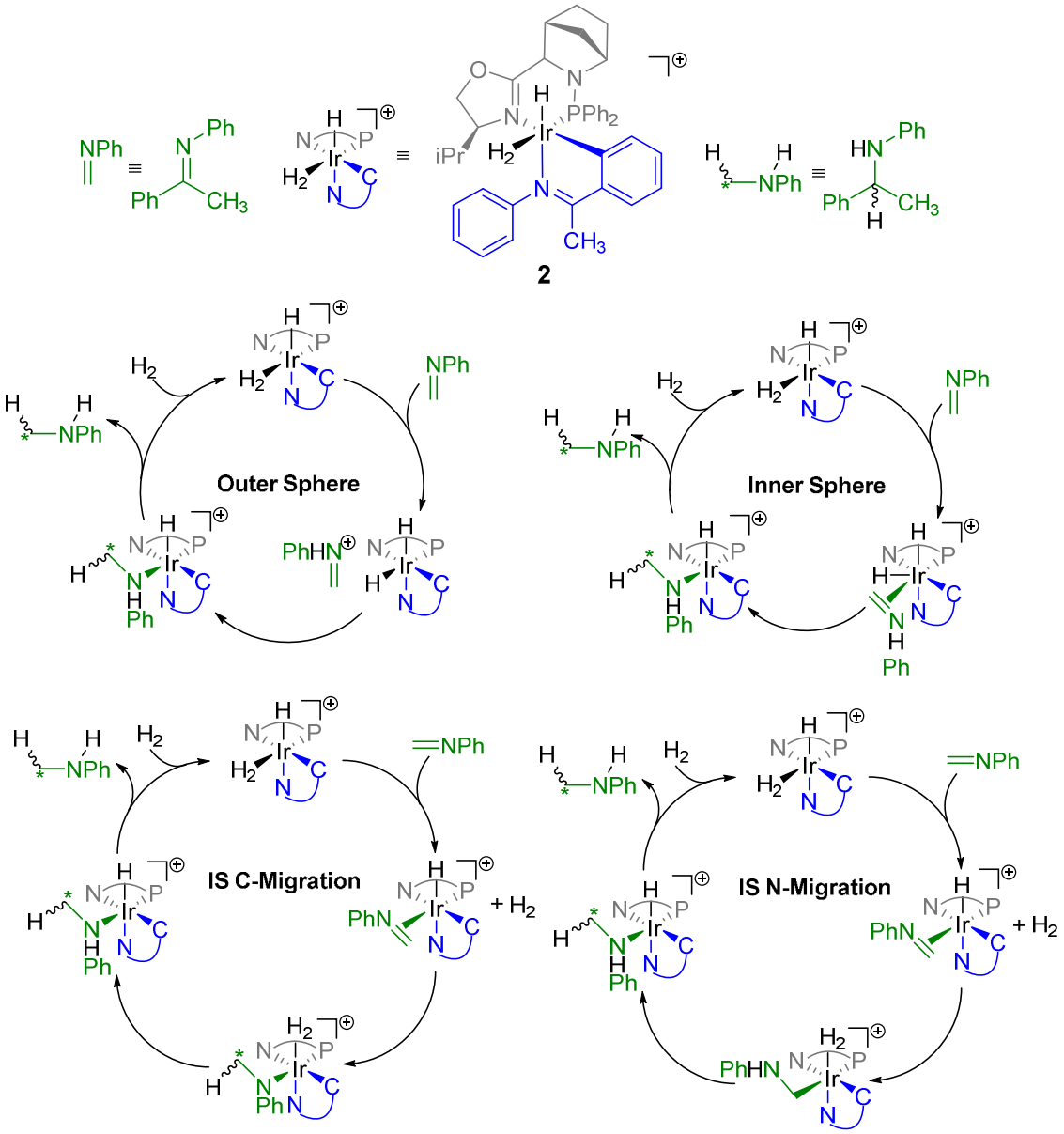

Scheme 1. Proposed catalytic cycles for imine hydrogenation using complex **2**: the outer sphere mechanism (upper left), the inner sphere mechanism through a heptacoordinated TS (upper right), the

inner sphere C-migration mechanism (lower left), and the inner sphere N-migration mechanism (lower right). * indicates a chiral center.

We started the investigation by calculating hydride transfer transition structures for a minimal model system. In this system, the Ir is part of a cyclometalated acrylimine in place of the full (*E*)-N,1-diphenylethan-1-imine substrate. A PH_3 was used in place of the phosphorus moiety of the Andersson ligand while NH_3 was used in place of the nitrogen portion of the Andersson ligand. As the small substrate model, we used formaldimine, which was protonated in some investigated mechanisms. Representative examples of both model and full system structures are provided in **Scheme 2**.

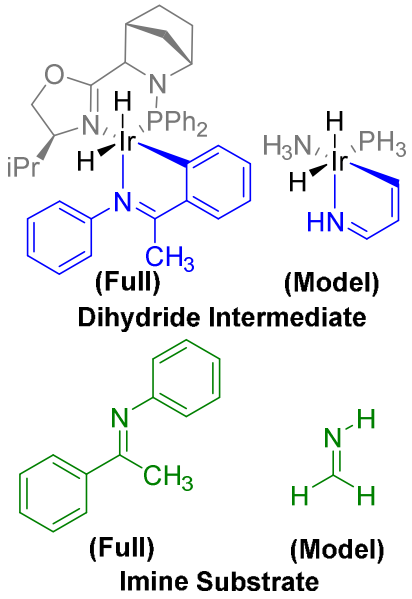

Scheme 2. Representative examples of full system structures and their corresponding model system structures.

Given its highly simplified nature, this model system does not describe sterics or stereoselectivity, but rather it is designed to provide general insights on the metal coordination and to potentially limit the number of coordination possibilities around the metal for each mechanism. Using this model system, all possible geometries of the hydride transfer transition states in each of the four mechanisms were calculated. This model data is referenced to a model version of low energy intermediate **7**, Table 1 (*vide infra*), where the amine product is coordinated to Ir. This is the product formed after the full hydrogenation of the substrate. One representative hydride transfer transition state geometry in each mechanism, except for the inner sphere through a heptacoordinated intermediate, is shown in **Figure 2**. Data for the remaining geometries calculated for each mechanism can be found in Table S1 in the

Supporting Information. A few basic trends can be noticed immediately from these model system data. First, the mechanism with the lowest energy hydride transfer transition states is the C-migration mechanism involving transition structures **5**, the lowest of which is structure **5a** at 82 kJ/mol. This stands in contrast to the previous results of Hopmann and Bayer,[15] who discounted a C-migration pathway due to high energy transition states. The second lowest energy transition structures are in the outer sphere pathway. The lowest energy transition structure of this pathway is **3d**, which is 26 kJ/mol higher than **5a**. The N-migration pathway proceeds via transition structures that are at least 60 kJ/mol higher in energy than the C-migration pathways. The energies for the few converged transition structures **4** that could be located for the inner sphere pathway through a heptacoordinated iridium intermediate were prohibitively high, as expected for a formal d20 complex. Therefore, this mechanism was not further explored.

For the other three mechanisms, we chose the two structures with the lowest energy or which mirrored the geometry around iridium of the crystal structures collected by Schramm and coworkers,[17] to calculate the diastereomeric transition structures of the experimentally studied system. For the outer sphere mechanism, these were structures **3a** and **3d**. For the C-migration mechanism, these were structures **5a** and **5b**. For the N-migration mechanism, these were structures **6a** and **6b**. Based on the model system results, these were determined to be the transition states most likely to match with experimental results and provide insight into the mechanism. Two coordination modes were observed by Schramm and coworkers for plausible intermediates.[17] Both fulfilled the expected requirement that ligands with strong trans influence/effect (carbanion, hydride, or phosphine) should not be trans to each other in a low energy complex. The same is true for all intermediates considered in our full systems, with the exception of the dihydride species in the outer sphere mechanism which has four ligands with high trans influence. We note that the “Halpern effect”, the preferences for some pathways to go via high energy intermediates, in several examples can be traced to a strong trans effect that is relieved in the subsequent transition state,[20] as is the case for the currently proposed outer sphere mechanism. Since the hydride transfer is the stereodetermining step for all mechanisms, the mechanism with the lowest energy hydride transfer transition state and that correctly reproduces the enantiomeric excess observed experimentally should be the overall favored pathway.

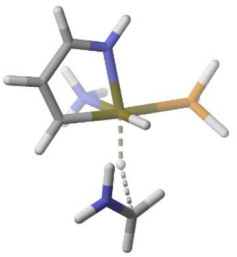

3d
108 kJ mol^{-1}

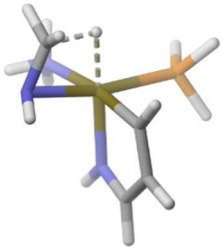

5a
82 kJ mol^{-1}

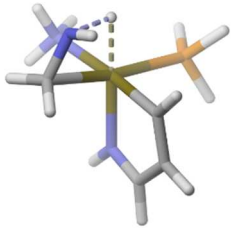

6a
142 kJ mol^{-1}

Figure 2. Representative examples of model system hydride transfer transition states

The possibility of crossovers between the proposed mechanisms was also considered. Of the four proposed mechanisms, the inner sphere mechanism through a heptacoordinated intermediate has already been rejected based on high energy transition structures in the model system and will not be discussed further here. Of the three remaining mechanisms, all three have the same starting structure: an Ir P,N complex with one hydride and cyclometalated imine substrate as shown in **Scheme 3**. The empty coordination site of this starting structure can be occupied by either H_2 or the π-bound substrate following the outer sphere or inner sphere pathways, respectively. These structures can only interchange by reverting to the initial starting structure that is common to all mechanisms, as can be shown by considering the possible pathways for crossover. In the outer sphere pathway, a proton transfer occurs with unbound substrate after coordination of H_2. The next step in the inner sphere pathways is, conversely, a hydride transfer to either the imine carbon or the imine nitrogen for the C- and N-migration pathways, respectively. At this stage, the intermediates have either a positively or a negatively

charged substrate-derived group on the Ir and are not directly in equilibrium with each other. The products of the C- and N-migration, both of which have negatively charged groups, have that charge localized on the nitrogen or on the carbon and are not directly in equilibrium either. After a hydride transfer in the outer sphere pathway and a proton transfer in the C- and N-migration pathways, the products obtained are the same for all three mechanisms. This analysis shows that it is highly unlikely, and likely impossible, for there to be crossover between the three proposed mechanisms mid-way through any pathway.

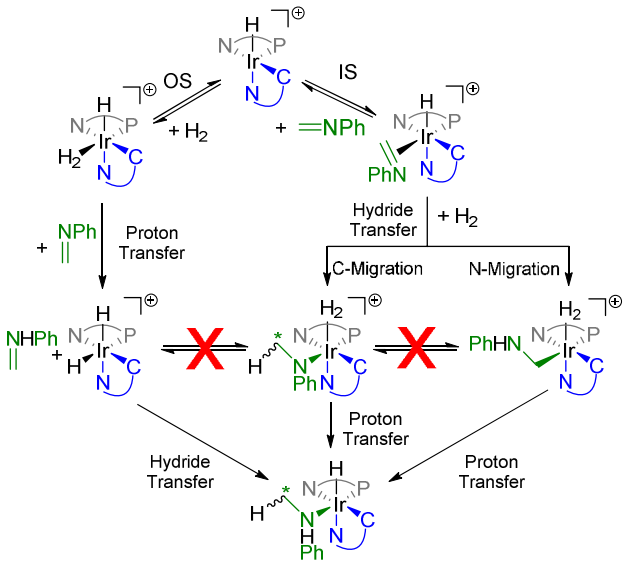

Scheme 3 Diagram of possible points of crossover between three proposed mechanisms. IS stands for 'inner sphere,' OS stands for 'outer sphere.'

We optimized the transition structures identified from the model system data for the three mechanisms using the full structures of an experimentally examined substrate and catalyst. The final energies for the lowest energy stereoisomers of each transition structure are shown in **Table 1** and are reported relative to the energy of the structure of the resting state of the catalyst with amine product bound to iridium, **7**.

Table 1. Structures and free energies for the full system catalyst resting state **7** and selected full system hydride transfer transition structures. Blue = N, orange = P, red = O, gold = Ir, dark grey = C, white = H. C-H hydrogens omitted for clarity.

	Outer Sphere			
Hydride Transfer TS Geometry	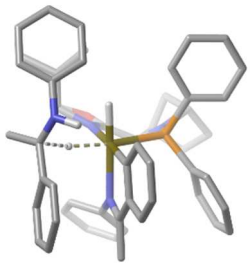	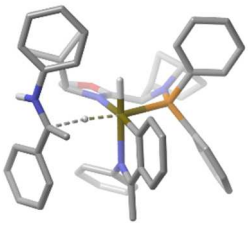	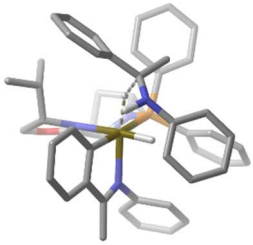	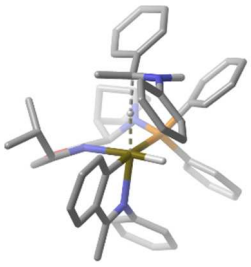
	3ar	**3as**	**3dr**	**3ds**
$\Delta G^{298\ K,DCM}$ [kJ/mol]	14	22	82	112
	Inner Sphere C-Migration			
Hydride Transfer TS Geometry	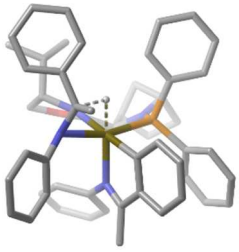	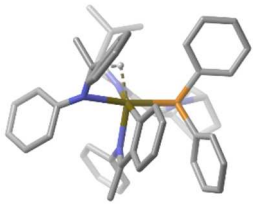	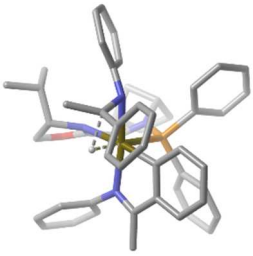	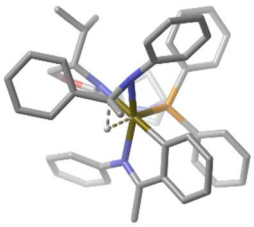
	5ar	**5as**	**5br**	**5bs**
$\Delta G^{298\ K,DCM}$ [kJ/mol]	89	108	104	119
	Inner Sphere N-Migration			
Hydride Transfer TS Geometry	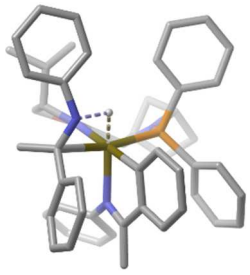	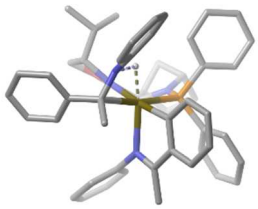	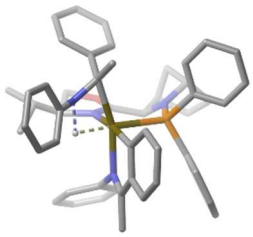	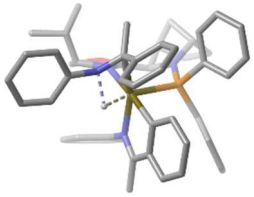
	6ar	**6as**	**6br**	**6bs**
$\Delta G^{298\ K,DCM}$ [kJ/mol]	157	177	225	225

Reference

$\Delta G^{298\ K,DCM}$ = 0 kJ/mol

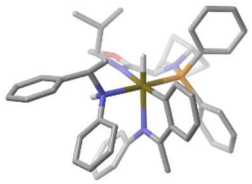

7

In order to gain insight into which of the three proposed pathways is the most favorable, the lowest energy diastereomeric transition structures for each of the three proposed mechanisms were compared. The lowest energy transition state of the outer sphere mechanism is the pro *R*, isomer **3ar** shown in Figure 3a. In comparison, the lowest energy structure of the inner sphere C-migration mechanism, the pro *R*, stereoisomer **5ar** shown in Figure 3b, is higher in energy by 75 kJ mol^{-1}. The lowest energy transition state of the inner sphere N-migration mechanism is the pro *R*, stereoisomer **6ar** shown in Figure 3c. Compared to **3ar**, the inner sphere N-migration mechanism is higher by 143 kJ mol^{-1} than the outer sphere alternative. These results suggest that the most favored mechanism has an iminium unbound to the iridium during the hydride transfer step in analogy to the results for the non-iridacycle pathway.[15]

A

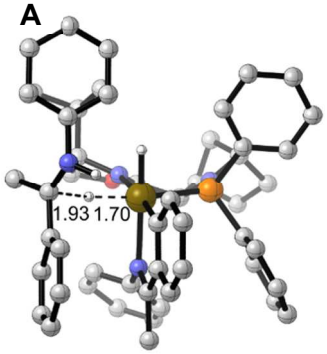

3ar
14 kJ mol^{-1}

B

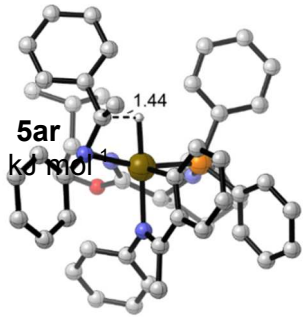

5ar
89 kJ mol^{-1}

C

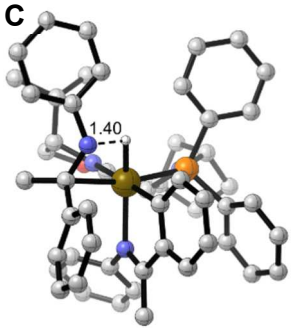

6ar
157 kJ mol^{-1}

Figure 3. Calculated structures for the lowest energy hydride transfer transition states of the three proposed mechanisms, a) outer sphere **3ar**, b) inner sphere C-migration **5ar**, and c) inner sphere N-migration **6ar**. C-H hydrogens omitted for clarity.

We next compared the lowest energy transition state in the outer sphere pathway, which results in an *R* product amine, **3ar** (Figure 4), to the lowest energy transition state in the same pathway which results in an *S* amine, **3as**. The transition state **3as** is 8 kJ/mol higher in energy than **3ar**. This leads to a prediction of 90% *ee* in favor of the *R* amine product, which is in excellent agreement with the experimental value of 90%. This agreement between calculation and experiment suggests that the outer sphere pathway via a cyclometalated Ir(III) complex is a good model for the reaction mechanism that can provide insights into the origin of the stereoselectivity.

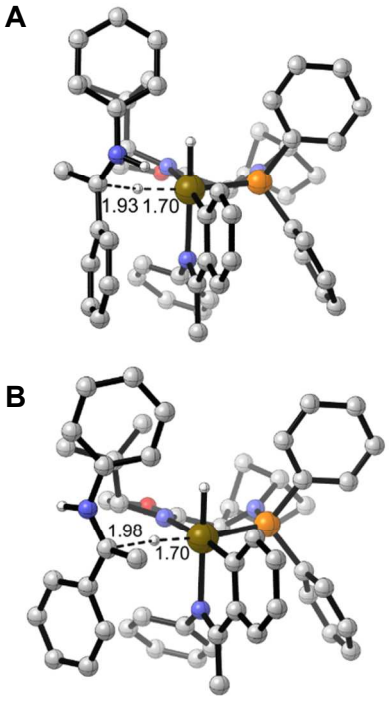

3ar
14 kJ mol^{-1}
Major

3as
22 kJ mol^{-1}
Minor

Figure 4. Calculated structures for the lowest energy hydride transfer transition states yielding a) *R* and b) *S* amine products in the iridium(III) inner sphere mechanism. C-H hydrogens omitted for clarity.

The finding that a reaction with good stereoselectivity proceeds via an outer sphere mechanism where the substrate is not coordinated to Ir and has only a single point of contact with the catalyst is surprising. Without multiple points of contact in the binding pocket of the catalyst, it would seem unlikely that the *i*Pr substituent on oxazoline could direct enantioselectivity by as much as it does (90%).

Before a more detailed analysis of the factors favoring the outer sphere pathway and the factors controlling stereoselectivity, control experiments to ensure that the same cyclometalated Ir complex forms and is the active species with the Andersson ligand, used in the comparison of the stereoselectivity, were performed. Using an *o*-Tol derivative of the ligand studied computationally, with $(o\text{-Tol})_2$ in place of Ph_2 on phosphorus, the hydrogenation reaction was run using cyclohexyl imine substrate **8**. This substrate was chosen as one for which cyclometalation would be difficult, if not impossible. A 0.5 mol% loading of COD-ligated catalyst precursor was added to a vial along with substrate and H_2 gas at either 20 or 50 bars pressure. The experiment was run twice at each of the two pressures, once without any additive and once with 5 mol% (*E*)-N,1-diphenylethan-1-imine. This additive was chosen as an imine implicated by Schramm and coworkers[17] to cyclometalate to Ir and form an active catalyst for hydrogenation. When no imine additive was included in the reaction mixture, conversion was low at both 20 bar (4% conversion) and 50 bar (5% conversion) after reaction at room temperature for 15 hours (Table 2, entries 1 and 2). Enantioselectivities were also quite low for these hydrogenations without additive, 18% and 15% *ee* at the two pressures, respectively. When the imine capable of forming the iridacycle catalyst was included as an additive (5 mol%), yields and enantioselectivities dramatically improved (Table 2, entries 3 and 4). This improvement strongly suggests the involvement of the iridacycle as the active catalyst for hydrogenation in the case of the Andersson ligand **1**. The cyclometalation of the additive is much faster than hydrogenation, given that the improvement of yield and stereoselectivity is observed when both additive and substrate are added at the same time. Additionally, a hydrogenation product derived from the additive was not observed along with hydrogenated substrate in reactions run with additive, providing further evidence for cyclometalation of the additive occurring to provide reaction improvement. Taken together, the results provide strong evidence that the mechanism involving the iridacycle is capable of explaining the high reactivity and stereoselectivity observed in the previous experiments[19] while the previously studied mechanisms[15] lacking its involvement are not. The previously proposed trihydride is conformationally labile in the presence of excess H_2, allowing a switch between two facial coordination geometries. Furthermore, the steric influence of the hydrides is negligible, allowing multiple approach vectors. Conversely, the configuration

around the metal in the iridacycle is locked analogous to the “chiral-at-metal” systems that lead to high stereoselectivities in a range of reactions by constraining possible approaches of the substrate.[21]

Table 2. Experimental results for hydrogenation run with and without cyclometalating imine additive.

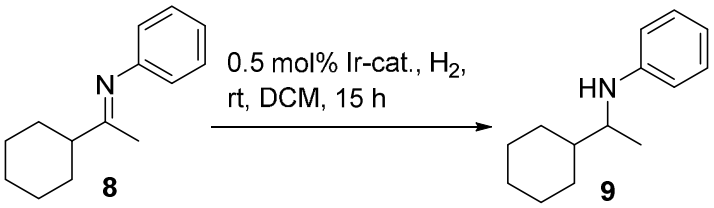

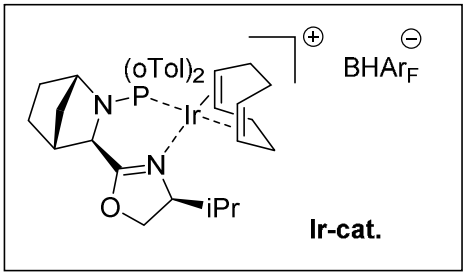

Entry	$p(H_2)$ (bar)	Additive	Conversion[a] (%)	ee[b] (%)
1	20	-	4	18 (*R*)
2	50	-	5	16 (*R*)
3	20	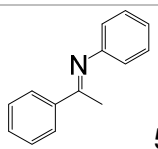 5 mol%	31	74 (*R*)
4	50		24	70 (*R*)

[a] Determined by NMR. [b] Determined by HPLC analysis on a Chiralcel-OJH column, 254 nm, hexane/iPrOH 98/2 or 99/1, 0.5 mL/min flow rate.

Having shown that the iridacycle mechanism is also applicable to the reaction under study here, the origin of the preference for the outer sphere mechanism and the origin of the surprisingly high stereoselectivity were analyzed in more detail. It can be noted that, for the iridacycle, an inner sphere mechanism involving proton transfer before hydride transfer would inevitably lead through a heptacoordinated intermediate. While such heptacoordinated Ir structures are precedented,[22] in the case of this mechanism, a heptacoordinated intermediate would be a sterically crowded, unfavorable 20-electron complex. Additionally, any inner sphere pathway would have the substrate held rigidly in place by the combination of the isopropyl group of the oxazoline ligand on one side and the cyclometalated imine on the other, thus restricting the ability of the substrate to relieve steric strain. In the outer sphere mechanism, the substrate can relieve this source of strain. This model is supported by an analysis of the C(Ph)-C=N-C(Ph)

dihedral angle of the iminium between the TSs of each mechanism (Table 3). The conjugated iminium system should have this dihedral at or close to 180°. Angles near 180° are observed for outer sphere TSs **3ar**, **3as**, **3dr**, and **3ds** (entries 1-4) but differ significantly from 180° for inner sphere mechanism structures (Table 3, entries 5-12). This indicates that, in the inner sphere mechanisms, the iminium must distort to relieve steric strain, something which is not necessary in the outer sphere pathway.

Table 3. C(Ph)-C-N-C(Ph) dihedral angles for reported TSs in each mechanism.

Entry	Structure	C(Ph)-C-N-C(Ph) Angle (°)	Entry	Structure	C(Ph)-C-N-C(Ph) Angle (°)
1	**3ar**	175.4	**7**	**5br**	134.2
2	**3as**	168.6	**8**	**5bs**	114.4
3	**3dr**	176.8	**9**	**6ar**	135.4
4	**3ds**	172.5	**10**	**6as**	126.2
5	**5ar**	116.3	**11**	**6br**	131.9
6	**5as**	125.3	**12**	**6bs**	46.6

Analysis of the relevant transition structures **3ar** and **3as** can provide insights into the structural original of the Gibbs free energy difference between them of 8 kJ/mol. Both **3ar** and **3as** have a similarly favorable C-H$\cdots\pi$ interaction between the *i*Pr C-H and the N-(Ph) group of the substrate (Figure 5a and c). The H-Ph(C) distance in **3ar** is 2.86 Å and in **3as** is 2.59 Å. However, **3ar** exhibits stacking interactions not present in **3as** (Figure 5b). The phenyl rings of the iminium substrate (C-Ph), the cyclometalated imine, and ligand stack in **3ar**, but not in **3as** (Figure 5b and c). Finally, in **3ar** the methyl group on the iminium carbon points towards the oxazoline, while in **3as** the phenyl group on the iminium carbon points towards the oxazoline, leading to additional steric strain in **3as**.

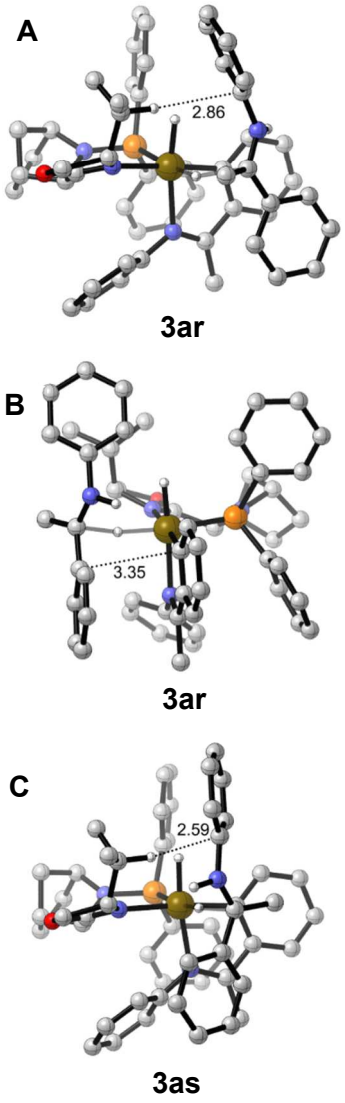

Figure 5. a) **3ar** side-on view showing distance (in Å) between oxazoline *i*Pr and substrate. b) **3ar** direct view showing distance (in Å) between phenyl groups aligned for aromatic stacking. c) **3as** side-on view showing distance (in Å) between oxazoline *i*Pr and substrate.

Conclusions

The iridium-catalyzed hydrogenation of imines is a powerful method for the generation of chiral amines. DFT calculations of the mechanism of imine hydrogenation using a realistic model of the Andersson iridium phosphine-oxazoline iridacycle catalyst suggest that the reaction proceeds through an outer sphere pathway. Experimental studies of a system that does not allow for the formation of the iridacycle lead to low reactivity and stereoselectivity, whereas substrates or additives that allow cyclometalation display significantly improved performance. The lowest energy hydride transfer transition structure for our outer sphere pathway is 75 kJ

mol^{-1} lower in energy than the lowest energy hydride transfer transition structure for the inner sphere C-migration pathway, and 143 kJ mol^{-1} lower in energy than the lowest energy hydride transfer transition state for the inner sphere N-migration pathway. The outer sphere pathway model predicts a 90% *ee* of *R* amine ($\Delta\Delta G^{\ddagger}$ = 8 kJ/mol) in excellent agreement with experiment for catalyst **2**. The origin of the stereoselectivity is traced to aromatic stacking interactions in the favored pathway.

The ability of the mechanism for hydrogenation proposed here to reconcile the contradictions found in the literature provides the basis for the development of improved chiral catalysts for the enantioselective hydrogenation of imines guided by a sound mechanism-guided analysis of candidate substrates and ligands. Previous work from our groups using the quantum-guided molecular mechanics (Q2MM) method[23] for the quantitatively accurate prediction of stereoselectivity of hydrogenation reactions provides a clearly defined roadmap for a high-throughput virtual screening of substrate/catalyst combinations for optimization of reaction outcomes. The transition structures elucidated in the present study provide the basis for the application of the Q2MM method to a catalytic reaction of significant interest in the pharmaceutical industry and other sectors of academia and industry.

Experimental Procedures

To an oven-dried pressure vial with magnetic stir bar, the imine (0.1mmol), additive (5 mol%) and iridium complex (0.5 mol%) in DCM (0.5 ml) were added. The vial was placed in a hydrogenation apparatus, purged three times with nitrogen then pressurized to 20 or 50 bar with hydrogen gas. After stirring 15 h, the pressure was released, and the solvent was evaporated to obtain yellow residual oil. The conversions were determined by ^{1}H NMR spectroscopy, and the *ee* values were determined by HPLC using a Chiralcel-OJH column, 254 nm, hexane/iPrOH 98/2 or 99/1, 0.5 mL/min flow rate.

Computational Methods

All calculations were performed using Gaussian 09.[24] All energies reported are Gibbs free energies, unless otherwise noted. Unconstrained geometry optimizations in the gas phase were performed using the M06 functional[25] with the sdd basis set[26] with effective core potentials (ECPs) for Ir and the 6-31G(d,p) basis set[27] for the other atoms. Grimme's D3 dispersion corrections[28] were included as a part of all calculations.[29] The single-point energies and solvent effects in DCM were computed based on the gas-phase optimized structures at the M06 level of

theory with the sdd basis set and ECPs for Ir and the 6-31G(d,p) basis set for the other atoms. Optimization in solution phase (DCM) resulted in no significant differences from the gas-phase calculations (see Supporting Information). Solvation energies were evaluated for the optimized geometries by a self-consistent reaction field (SCRF) using the SMD model.[30] Frequency calculations performed in the gas phase confirmed the stationary points as transition states (one imaginary frequency) or minima (no imaginary frequencies). Transition states were further characterized by intrinsic reaction coordinate (IRC) calculations.[31] In the case of small energy differences between transition states and related intermediates, IRC calculations systematically failed. In such situations, 'quick reaction coordinate' (QRC) calculations were performed.[32] This method involves performing a small manual displacement (0.25 bohr) of the geometry on the vibration of the imaginary frequency followed by optimization to a minimum. The final free energies were calculated by adding the single-point energies of the structures calculated with the implicit solvent model to the thermal corrections from the gas phase optimizations. The results for all of the structures are presented in Table S2. The final free energies from the optimizations are reported in kJ/mol. Figures 2 - 5 and the structures in Table 1 were created using CYLview.[33]

Supporting Information

All energies (electronic, free energies, ZPE), single imaginary frequencies, and Cartesian coordinates for all complexes and transition states discussed. This material is available free of charge via the Internet at http://pubs.acs.org.

Acknowledgments

We would like to thank the National Science Foundation (CHE-1565669), the Swedish Research Council (VR), the Stiftelsen Olle Engkvist Byggmästare, and the Swedish Energy Agency for support of this research, and the National Science Foundation for providing B.T. with financial support through the IRES program (OISE-1261033).

References

[1] (a) *Chiral Amine Synthesis: Methods, Developments, and Applications.* (Ed.: Nugent, T. C.) Wiley-VCH, Weinheim, **2010**. (b) Xie, J.-H.; Zhu, S.-F.; Zhou, Q.-L. *Chem. Rev.* **2011**, *111*, 1713-1760.

[2] (a) Crabtree, R. H.; Felkin, H.; Morris, G. E. *J. Organomet. Chem*., **1977**, *141*, 205-215. (b) Crabtree, R. H.; Morris, G. E. *J. Organomet. Chem.*, **1977**, *135*, 395-403. (c) Crabtree, R. H.; Felkin, H.; Fillebeen-Khan, T.; Morris, G. E. *J. Organomet. Chem*., **1979**, *168*, 183-195. (d) Crabtree, R. *Acc. Chem. Res*., **1979**, *12*, 331-337. (e) Crabtree, R. H.; Demou, P. C.; Eden, D.; Mihelcic, J. M.; Parnell, C. A.; Quirk, J. M.; Morris, G. E. *J. Am. Chem. Soc*., **1982**, *104*, 6994-7001. (f) Crabtree, R. H.; Uriarte, R. J. *Inorg. Chem*., **1983**, *22*, 4152-4154. (g) Chin, C. S.; Lee, B. *J. Chem. Soc., Dalton Trans*., **1991**, 1323-1327.

[3] Schnider, P.; Koch, G.; Prétôt, R.; Wang, G.; Bohnen, F. M.; Krüger, C.; Pfaltz, A. *Chem. - Eur. J.* **1997**, *3*, 887-892.

[4] (a) Helmchen, G.; Pfaltz, A. *Acc. Chem. Res*., **2000**, *33*, 336-345. (b) Pfaltz, A.; Blankenstein, J.; Hilgraf, R.; Hörmann, E.; McIntyre, S.; Menges, F.; Schönleber, M.; Smidt, S. P.; Wüstenberg, B.; Zimmermann, N. *Adv. Synth. Catal*., **2003**, *345*, 33-43. (c) Wang, D.-S.; Chen, Q.-A.; Lu, S.-M.; Zhou, Y.-G. *Chem. Rev*., **2012**, *112*, 2557-2590. (d) Cadu, A.; Andersson, P. G. *Dalton Trans*., **2013**, *42*, 14345-14356. (e) Verendel, J. J.; Pàmies, O.; Diéguez, M.; Andersson, P. G. *Chem. Rev*., **2014**, *114*, 2130-2169.

[5] Mazet, C.; Smidt, S. P.; Meuwly, M.; Pfaltz, A. *J. Am. Chem. Soc.,* **2004**, *126*, 14176-14181.

[6] (a) Zhu, S.-F.; Xie, J.-B.; Zhang, Y.-Z.; Li, S.; Zhou, Q.-L. *J. Am. Chem. Soc*., **2006**, *128*, 12886-12891. (b) Hedberg, C.; Källström, K.; Brandt, P.; Hansen, L. K.; Andersson, P. G. *J. Am. Chem. Soc*., **2006**, *128*, 2995-3001.

[7] Trifonova, A.; Diesen, J. S.; Andersson, P. G. *Chem. - Eur. J.*, **2006**, *12*, 2318-2328.

[8] Hopmann, K. H.; Bayer, A. *Coord. Chem. Rev*. **2014**, *268*, 59-82.

[9] (a) Baeza, A.; Pfaltz, A. *Chem. - Eur. J.*, **2010**, *16*, 4003-4009. (b) Guiu, E.; Claver, C.; Benet-Buchholz, J.; Castillón, S. *Tetrahedron: Asymmetry*, **2004**, *15*, 3365-3373.

[10] (a) Tani, K.; Onouchi, J.-I.; Yamagata, T.; Kataoka, Y. *Chem. Lett.* **1995**, *91*, 955-956. (b) Moessner, C.; Bolm, C. *Angew. Chem., Int. Ed.* **2005**, *44*, 7564-7567. (c) Mršić, N.; Minnaard, A. J.; Feringa, B. L.; de Vries, J. G.; *J. Am. Chem. Soc.* **2009**, *131*, 8358-8359.

[11] (a) Church, T. L.; Rasmussen, T.; Andersson, P. G. *Organometallics*, **2010**, *29*, 6769-6781. (b) Mazuela, J.; Norrby, P.-O.; Andersson, P. G.; Pàmies, O.; Diéguez, M. *J. Am. Chem. Soc*., **2011**, *133*, 13634-13645. (c) Fan, Y.; Cui, X.; Burgess, K.; Hall, M. B. *J. Am. Chem. Soc*. **2004**, *126*, 16688-16689. (d) Cui, X.; Fan, Y.; Hall, M. B.; Burgess, K. *Chem. - Eur. J.* **2005**, *11*, 6859-6868. (e) Sparta, M.; Riplinger, C.; Neese, F. *J. Chem. Theory Comput*., **2014**, *10*, 1099-1108.

[12] (a) Martín, M.; Sola, E.; Tejero, S.; Andrés, J. L.; Oro, L. A. *Chem. - Eur. J.* **2006**, *12*, 4043-4056. (b) Martín, M.; Sola, E.; Tejero, S.; López, J. A.; Oro, L. A. *Chem. - Eur. J.* **2006**, *12*, 4057-4068.

[13] Samec, J. S. M.; Bäckvall, J.-E.; Andersson, P. G.; Brandt, P. *Chem. Soc. Rev.*, **2006**, *35*, 237-248.

[14] Fabrello, A.; Bachelier, A.; Urrutigoïty, M.; Kalck, P. *Coord. Chem. Rev*., **2010**, *254*, 273-287.

[15] Hopmann, K. H.; Bayer, A. *Organometallics* **2011**, *30*, 2483-2497.

[16] (a) Sandoval, C. A.; Ohkuma, T.; Muñiz, K.; Noyori, R. *J. Am. Chem. Soc*., **2003**, *125*, 13490-13503. (b) Bartoszewicz, A.; Miera, G. G.; Marcos, R.; Norrby, P.-O.; Martín-Matute, B. *ACS Catal.* **2015**, *5,* 3704-3716.

[17] Schramm, Y.; Barrios-Landeros, F.; Pfaltz, A. *Chem. Sci.,* **2013**, *4*, 2760-2766.

[18] (a) Chen, H.-Y. T.; Wang, C.; Wu, X.; Jiang, X.; Catlow, C. R. A.; Xiao, J. *Chem. - Eur. J.*, **2015**, *21*, 16564-16577. (b) Tang, W.; Lau, C.; Wu, X.; Xiao, J. *Synlett*, **2014**, *25*, 81-84.

[19] (a) Brandt, P.; Hedberg, C.; Andersson, P. G. *Chem. - Eur. J.* **2003**, *9*, 339-347. (b) Trifonova, A.; Diesen, J. S.; Chapman, C. J.; Andersson, P. G. *Org. Lett*., **2004**, *6*, 3825-3827.

[20] Landis, C. R.; Halpern, J. *J. Am. Chem. Soc*., **1987**, *109*, 1746-1754.

[21] (a) Xu, W.; Arieno, M.; Löw, H.; Huang, K.; Xie, X.; Cruchter, T.; Ma, Q.; Xi, J.; Huang, B.; Wiest, O.; Gong, L.; Meggers, E. *J. Am. Chem. Soc*., **2016**, *138*, 8774-8780. (b) Tutkowski, B.; Meggers, E.; Wiest, O. *J. Am. Chem. Soc.*, **2017**, *139*, 8062-8065. (c) Huang, X.; Quinn, T. R.; Harms, K.; Webster, R. D.; Zhang, L.; Wiest, O.; Meggers, E. *J. Am. Chem. Soc.*, **2017**, *139*, 9120-9123.

[22] (a) Housecroft, C. E. Iridium: Inorganic & Coordination Chemistry. *Encyclopedia of Inorganic Chemistry*, Vol. 43; Wiley, **2006**. (b) Loza, M.; Faller, J. W.; Crabtree, R. H. *Inorg. Chem*., **1995**, *34*, 2937-2941.

[23] Hansen, E.; Rosales, A. R.; Tutkowski, B.; Norrby, P.-O.; Wiest, O. *Acc. Chem. Res*., **2016**, *49*, 996-1005.

[24] Frisch, M. J.; Trucks, G. W.; Schlegel, H. B.; Scuseria, G. E.; Robb, M. A.; Cheeseman, J. R.; Scalmani, G.; Barone, V.; Mennucci, B.; Petersson, G. A.; *et al*. Gaussian, Inc., Wallingford CT, 2009.– please see Supporting Information reference 1

[25] Zhao, Y.; Truhlar, D. G. *Theor. Chem. Acc*. **2008**, *120*, 215-241.

[26] Dunning Jr., T. H.; Hay, P. J. in *Modern Theoretical Chemistry*, Ed. H. F. Schaefer III, Vol. 3 Plenum: New York, 1977; pp 1-28.

[27] Hehre, W. J.; Radom, L.; Schleyer, P. v. R.; Pople, J. A. *Ab Initio Molecular Orbital Theory*; Wiley: New York, 1986.

[28] Grimme, S.; Antony, J.; Ehrlich, S.; Krieg, H. *J. Chem. Phys*. **2010**, *132*, 154104-154119.

[29] Averkiev, B. B.; Zhao, Y.; Truhlar, D. G. *J. Mol. Catal. A: Chem*., **2010**, *324*, 80-88.

[30] Marenich, A. V.; Cramer, C. J.; Truhlar, D. G. *J. Phys. Chem. B*, **2009**, *113*, 6378-6396.

[31] (a) Fukui, K. *Acc. Chem. Res*. **1981**, *14*, 363-368. (b) Hratchian, H. P.; Schlegel, H. B. *J. Chem. Phys*. **2004**, *120*, 9918-9924. (c) Hratchian, H. P.; Schlegel, H. B. In *Theory and Applications of Computational Chemistry: The First 40 Years*; Dykstra, C. E., Frenking, G., Kim, K. S., Scuseria, G., Eds.; Elsevier: Amsterdam, 2005; p 195. (d) Hratchian, H. P.; Schlegel, H. B. *J. Chem. Theory Comput*. **2005**, *1*, 61−69.

[32] Goodman, J. M.; Silva, M. A. *Tetrahedron Lett.* **2003**, *44*, 8233-8236.

[33] Legault, C. Y. *CYLview, 1.0b*; Université de Sherbrooke, Sherbrooke, Quebec, Canada, 2009; http://www.cylview.org (accessed May 15, 2017).